Magnetic field gradients from the ST-5 constellation: Improving magnetic and thermal models of the lithosphere

M. Purucker[1], T. Sabaka[1], G. Le[2], J. A. Slavin[2], R. J. Strangeway[3], and C. Busby[4]

[1]Raytheon at Planetary Geodynamics Laboratory, NASA Goddard Space Flight Center, Greenbelt, MD 20771

[2]Heliophysics Sciences Division, NASA Goddard Space Flight Center, Greenbelt, MD 20771

[3]Institute of Geophysics and Planetary Physics, University of California, Los Angeles, CA 90024-1567

[4]Dept of Earth Sciences, University of California-Santa Barbara, Santa Barbara, CA 93106-9630

Abstract

We report the development of a new technique (magnetic gradiometry) for satellite-based remote sensing of the lithosphere. The measurements reported here represent the first systematic measurements of lithospheric magnetic field gradients, and were collected from a spinning spacecraft. The three-satellite ST-5 mission collected vector magnetic field observations at 300-800+ km altitudes over mid and high-northern latitudes in 2006. Away from the auroral oval, and over the continents, the gradients of the low altitude (<400 km) total anomaly field are dominated by lithospheric magnetic fields. Using a seismic starting model, and magnetic field observations from ST-5 and other recent satellite missions, we demonstrate how these techniques can be used to improve our knowledge of the processes involved in the thickened crust of the Colorado Plateau and the Sierra Madre Occidental.

Background

The launch of the Space Technology 5 (ST-5) constellation on 22 March 2006 lofted three satellites whose only scientific instruments consisted of boom-mounted vector fluxgate magnetometers. For an overview of the mission, and the performance of the magnetometers, the reader is directed to Slavin et al. (2007).

Satellite constellations enable the efficient collection of in situ measurements over large volumes of space. In the case of the magnetic field, constellations enable the separation of temporal from spatial effects. Our approach has been to remove temporal effects by sampling the magnetic field at the same instant from spacecraft separated by a distance comparable to their altitude above the surface. The European Space Agency has under development Swarm, a three-satellite constellation (Olsen et al., 2006) that will make high-precision magnetic field measurements. Although both the ST-5 and Swarm constellations are designed to map the Earth's magnetic field, they employ radically different design approaches. The merits and drawbacks of these approaches are further reviewed in the discussion.

New gradient observations

The ST-5 spacecraft are spin-stabilized (20 rpm), and the sun sensor achieved accuracies of 0.1-0.3 degrees relative to the spacecraft body. Because of the dawn-dusk orbit, the sun sensors have a view of the sun throughout each orbit. Lacking a GPS, the spacecraft locations were determined via tracking with location accuracies of 1-10 km or better. The

largest errors are at perigee with along-track errors > vertical errors > cross-track errors.

A 1 km orbit error (Langel and Hinze, 1998) translates into, at most, a 28 nT field magnitude error if the error is vertical, 6 nT if the error is along track, and 5 nT if across track. Orbit determination solutions until 3 May 2006 were based on propagating one orbit solution per day. After 3 May the orbit solutions were propagated for 2-3 days. As will be demonstrated in this paper, field magnitude and gradient errors are considerably smaller than expected until 3 May. A magnetic cleanliness program, and preflight calibration at the GSFC magnetic test facility, ensured that spacecraft fields amounted to less than 1 nT at the magnetometer location. Data processing involved in-flight calibration, and despinning the data into an inertial coordinate system (Slavin et al., 2007). The in-flight calibration was against the current, spherical harmonic degree 13, International Geomagnetic Reference Field (IGRF) (Macmillan and Maus, 2005). The gradients are calculated by first determining the total anomaly field (Δ T) from each spacecraft

$$\Delta T = \hat{\mathbf{F}} \cdot \mathbf{T}$$

where $\hat{\mathbf{F}}$ is the unit vector in the direction of **F,** the magnitude of the (largely) non-crustal IGRF field and **T** is the residual field vector after removal of the IGRF field. The gradient ($\hat{G}$) is then calculated by differencing these total field anomaly measurements from the nearby spacecraft at the same instant in time, normalized by the interspacecraft distance (d). The gradient is thus defined as

$$\hat{G} = (\Delta T_1 - \Delta T_2) / d$$

where the subscript indicates the spacecraft.

We report here only the gradient measurements between the two trailing spacecraft (094 and 224) of the constellation because their separation distance was comparable to their altitude. In contrast, the leading spacecraft (155) had much larger separations, up to 5000 km, from the two trailing spacecraft. The ST-5 gradient data for the two trailing spacecraft consist of 726158 observations at altitudes below 800 km (the approximate limit for lithospheric field sensing), and are available at http://geodynamics.gsfc.nasa.gov/research/purucker/st5_gradients.html

Results

The gradient measurements were validated by comparison with the Comprehensive (CM4) field model (Sabaka et al., 2004), a model of the quiet-time, near-Earth magnetic field which includes internal and external sources, associated induced contributions, and toroidal magnetic fields. CM4 was derived using data from satellite mapping missions (Ørsted, CHAMP, Magsat, and POGO), and ground-based observatories. The CM4 field used for comparison was the high degree (14-60) static total anomaly field of internal origin, representing largely fields of lithospheric origin. The period of time encompassing the ST-5 flight was magnetically quiet, with 66 of the 90 days of the mission having periods with $K_p <= 1^o$.

The comparison entailed calculating the linear correlation coefficient (Press et al., 1996), with a correlation coefficient (r) of 1 representing perfect correlation, 0 representing no correlation, and –1 representing perfect anti-correlation. These correlation coefficients

were based on all low altitude data (< 400 km) from the mission. The data were first assembled into bins measuring 10 degrees in latitude by 20 degrees in longitude in non-polar regions, and correspondingly larger in the polar regions. The measured gradients shown in Figure 1a represent low altitude (< 400 km) measurements from the ST-5 mission that exhibit a correlation coefficient in excess of 0.5. Away from the auroral oval, and over the continents, the gradients are dominated by lithospheric magnetic fields, and commonly exhibit correlations of between 0.5 and 0.9 with the previously determined lithospheric field from CM4. The difference between continental and oceanic correlation coefficients is expected because continental magnetic fields of lithospheric origin are usually stronger than oceanic magnetic fields by a factor of two or more (Maus et al., 2007). This difference was not recognized from the Magsat results (Langel and Hinze, 1998) because of Magsat's higher noise levels compared with CHAMP. The appearance of this difference in the ST-5 results suggests that the quality of the data, for lithospheric field studies, is superior to that from Magsat. Although the quality of the ST-5 results is high, there exist significant biases between the observed and predicted gradients, which we ascribe, in part, to orbit errors. The linear correlation coefficient is not very sensitive to the presence of these biases. These biases can be seen by comparing Figures 1a and 1c, the maps of the observed and predicted gradients. These biases become especially noticeable after 3 May 2006, when the orbit determination became less reliable. We have made a preliminary correction of these biases in the ST-5 gradient data by calculating, for each spacecraft, and for each pass, a median offset between the predicted and observed total anomaly field when the spacecraft is outside of the auroral zone. Applying this correction results in Figure 1b, which shows a much stronger visual

comparison with the predicted gradient. However, after May 15 we find that a bias correction alone is insufficient.

Further comparisons were made to individual magnetic features measured over southern North America (Figure 2), again by comparison to CM4. These comparisons are between the corrected gradients discussed above, and the predicted ones. The Kentucky magnetic anomaly (Figure 2, top row), a manifestation of the magnetic edge of cratonic North America (Purucker et al., 2002), and local enhancements of magnetization, stands out clearly. The magnitude of the total field anomaly, up to 46 nT at 305 km altitude (Figure 2, upper left), is nearly a factor of two larger than seen on previous magnetic mapping missions. This enhancement is attributed to the lower altitude of ST-5. The measured interspacecraft difference field ($\hat{G} * d$) compares well with that predicted by CM4 (Figure 2, upper center figures). The map of the measured minus predicted field (Figure 2, upper right) shows little pass to pass structure that is coherent. Over southwestern North America (Figure 2, bottom row), the largest positive total field anomaly is again associated with the magnetic edge of cratonic North America (Purucker et al.,2002). The measured interspacecraft difference field ($\hat{G} * d$) also compares well with that predicted by CM4 (Figure 2, lower center figures). The difference map between the measured and predicted fields (Figure 2, lower right) shows pass to pass structure that is coherent in the El Paso-Delaware basin region, and in NW Sinaloa State, Mexico, among other places. These are areas in which the ST-5 data could improve upon existing magnetic fields models.

Joint seismic-magnetic model

Global magnetization models represent an integration of compositional and thermal models of the crust and mantle with crustal magnetic field measurements from satellite. We have previously used (Fox Maule et al., 2005) the 3SMAC (Nataf and Ricard, 1996) compositional and thermal model of the crust and mantle as a starting model, and modified it in an iterative fashion with the satellite data until the magnetic field predicted by the model matches the observed magnetic field. A unique magnetic crustal thickness solution is obtained by assuming that induced magnetizations dominate in continental crust, using a model to describe the oceanic remanence, and assuming that vertical thickness variations dominate over lateral susceptibility variations. A starting model is necessary to constrain wavelengths obscured by overlap with the core field (Spherical harmonic degrees 1-14), and to ensure that most magnetic crustal thicknesses will be non-negative.

The model-making procedure is as follows: The total anomaly field is calculated from this starting model under the assumption of a constant magnetic susceptibility of 0.04 SI, and long wavelength fields (spherical harmonic degree < 15) are removed, simulating a main field removal. The observed and modeled satellite fields are differenced, and the difference is converted to a magnetic crustal thickness. The starting model is then updated to reflect this change, and the process continues until the predicted magnetic field reproduces the observed field at the level desired. The process is non-linear because the total anomaly field is used, and because of the high-pass filter. Our crustal thickness codes and models are available at http://planetary-mag.net/crustal_thickness_codes.

Instead of using the ST-5 field or gradient measurement directly, we base the following analysis on the MF-5 crustal field model (Maus et al., 2007). We do this for two reasons: 1) our analysis requires a global data set, and 2) some unmodeled external fields remain in the ST-5 data. MF-5 is constructed from six years of CHAMP satellite data, and includes spherical harmonic terms up to degree and order 100 (wavelength = 400 km).

Subsequent to the publication of 3SMAC and our initial investigations, improved seismic models of North America (Chulick and Mooney, 2002) have become available which we use here to locally improve the global starting model. The crustal thickness (without including sediments) was extracted (Figure 3, center, shows their distribution and the inferred crustal thickness) from this model, binned and averaged in two degree blocks, and then a surface of continuous curvature with tension = 0.35 was fit to the averages. This allows for a direct comparison with 3SMAC and our magnetization model, both of which are developed on a two degree grid. The final magnetic crustal thickness over SW North America calculated using this starting model, updated using the MF-5 magnetic model, is shown in Figure 3 (right), with residuals between predicted and observed magnetic fields of less than 0.5 nT.

Discussion

The magnetic thickness map clearly shows the SW edge of the thickened crust of the Great Plains, the thickened crust under the Colorado Plateau, the relatively thinned crust between these two areas in which the Rio Grande rift is located, and the thin crust of the

Gulf of California. All of these are in agreement with the seismically determined thicknesses summarized in Chulick and Mooney (2002), and with other compilations. The thickest parts of the Colorado Plateau crust are in the middle of the Colorado Plateau, in northernmost Arizona and SE Utah, and average about 45 km. These areas correspond to the highest, and most uniform, topography on the Plateau, in contrast to the higher relief prevalent in most of Utah. This provides some support for theories which relate the uplift to crustal thickening. While the magnetic approach is incapable of the spatial resolution of the seismic technique, it offers a 2-D view which can only be duplicated by multiple seismic surveys. An alternative interpretation of the magnetic field observations would relate them to enhanced magnetic susceptibilities (Hemant and Maus, 2005). This in turn implies compositional differences between the Colorado Plateau crust and surrounding regions. However, crustal compositions, as inferred from seismic velocities by Parsons et al. (1996), appear to be the same beneath the Colorado Plateau and the Basin and Range Province to the southwest, suggesting that magnetic thickness variations dominate over susceptibility variations in this region. The coherent differences between the measured and modeled ST-5 gradients over the Delaware Basin-El Paso region (Figure 2, lower right) suggest that ST-5 is seeing shorter wavelength features of the crust, possibly associated with the development of the Rio Grande rift in this region.

Other prominent features that are not well resolved in the seismic thickness map include the thickened crust in Baja California and in Mexico's Sierra Madre Occidental. The thickened crust under the Sierra Madre Occidental is especially intriguing, as it coincides in part with an areally extensive and thick ignimbrite (Ferrari et al., 2002) of Oligocene

and early Miocene age (Figure 3). In particular, that part of the ignimbrite field unaffected by Tertiary extension forms the SW boundary of the magnetically thick crust in this region. The ignimbrite field has been related to detachments of the subducted Farallon slab in Miocene time which in turn controlled the locus and timing of volcanism (Ferrari et al., 2002). The magnetic thickness results here could be interpreted in terms of basaltic underplating associated with these hypothetical detachment events, and might further be interpreted to mean that the crust here was thickened by batholiths beneath the ignimbrite field, and in the south and west was thinned by extension in the Miocene. The coherent differences between the measured and modeled ST-5 gradients over NW Sinaloa State, Mexico (Figure 2, lower right) suggest that ST-5 is seeing shorter wavelength features of the crust, possibly associated with Miocene extension or the opening of the Gulf of California in this region.

Bounds on the ephemeris error of the ST-5 orbit can be estimated from the residual statistics of the total anomaly field. As can be seen from Figure 1, non-lithospheric fields dominate at high magnetic latitudes. Far-field effects of the polar electrojet can be seen to magnetic latitudes as low as 50 degrees (Maus et al., 2007). This is evident in the calculated RMS values of the total anomaly field residuals (Table 1), which are about 12 nT when considering magnetic latitudes equatorward of 50 degrees. This implies an RMS tracking accuracy of better than 2-3 km at perigee, if the orbit errors are primarily along-track. The RMS residual of interspacecraft difference data $\hat{G} * d$ is considerably less (Table 1), about 6 nT. We identify two reasons for this improved RMS misfit relative to that associated with the total anomaly field. First, location errors will be correlated

between the two nearby ST-5 spacecraft because they are identical, have almost identical pointing, and would be expected to experience very similar drag histories. This introduces a serial correlation of the errors. Second, the gradient measurement suppresses the longer wavelength features at the expense of shorter wavelength features.

Improvements in the ST5 measured fields, and associated gradients, could be achieved by improving the ephemeris information. This has been possible in a deterministic sense as discussed in the previous section. It might also be possible in a stochastic sense using a Brownian Bridge algorithm (Jackson et al., 2000). In this approach, the satellite is assumed to have a fixed (and known) position at times of range determination. The position errors, and the covariance of those errors, grow and decay with time as a function of distance from those range determination locations.

Historically, spinning spacecraft have been seen as unsuitable platforms for performing scientific-quality geomagnetic observations (Langel and Hinze, 1998) because of imprecise knowledge of the attitudes of the magnetometer's axes. A star tracker is capable of improving on attitude knowledge accuracy by more than an order of magnitude relative to a sun sensor. This results in an absolute accuracy for the vector components of a few nT. However, some fields within geomagnetism, such as lithospheric field studies, are not as dependent on precise knowledge of the attitudes of the magnetometer's axes. With the exception of narrow bands around the magnetic dip equator, measurement of the total magnetic field anomaly is sufficient for proper interpretation and reconstruction of the vector field (Purucker, 1990). It is important to

point out that lithospheric field studies on ST-5 have benefited enormously from flying at Solar Minimum, and from the strict magnetic cleanliness program. But the conclusion remains the same. The measurement of lithospheric fields nearly a factor of two larger than on previous magnetic mapping missions, and their interpretation, has been possible without precise pointing knowledge. The 3-axes stabilized spacecraft traditionally used for geomagnetic observations of the lithospheric field (CHAMP, and the upcoming Swarm mission) are large, heavy spacecraft, with masses averaging more than 500 kg each, in contrast to the 25 kg ST-5 spacecraft. It is hoped that further technical advances in the area of star trackers will reduce the need for 3-axes stabilization.

Acknowledgments

We would like to acknowledge the ST-5 team, and NASA, for support of this work. The manuscript was improved by reviews from Stefan Maus and Manoj Nair.

Reference list

Chulick, G.S. and W.D. Mooney (2002) Seismic structure of the Crust and Uppermost Mantle of North America and adjacent oceanic basins: A Synthesis, *Bull. Seis. Soc. Amer*., 92(6), 2478-2492.

Ferrari, L., M. Lopez-Martinez., and J. Rosas-Elguera (2002) Ignimbrite flare-up and deformation in the southern Sierra Madre Occidental, western Mexico: Implications from the late subduction history of the Farallon plate, *Tectonics*, 21(4),1-24.

Fox Maule, C., M. Purucker, N. Olsen, and K. Mosegaard (2005) Heat flux anomalies in Antarctica revealed by satellite magnetic data, *Science*, 309, 464-467.

Hemant K., and S. Maus (2005) Geological modeling of the new CHAMP magnetic anomaly maps using a geographical information system technique, *J. Geophys. Res*., 110, B12103, doi:10.1029/2005JB003837.

Hunt, C.B. (1956) Cenozoic Geology of the Colorado Plateau, *U.S. Geol. Survey Prof. Paper* 279, Washington, DC, 99 pp.

Jackson, A, A. Jonkers, and M. Walker (2000) Four centuries of geomagnetic secular variation from historical records, *Phil. Trans. R. Soc. London*, 358, 957-990.

Langel, R.A. and W. J. Hinze (1998) *The Magnetic Field of the Earth's Lithosphere: The satellite perspective*, 429 pp, Cambridge University Press.

Macmilan, S, and S. Maus (2005) International Geomagnetic Reference Field – the tenth generation, *Earth, Planets and Space*, 57(12), 1135-1140.

Maus, S., H. Lühr, M. Rother, K. Hemant, G. Balasis, P. Ritter, and C. Stolle (2007) Fifth generation lithospheric magnetic field model from CHAMP satellite measurements, *Geochem. Geophys. Geosyst*., 8, Q05013, doi:10.1029/2006GC001521.

Nataf, H., and Y. Ricard (1996) 3SMAC: An a priori tomographic model of the upper mantle based on geophysical modeling, *Phys. Earth Plan. Int*., 95, 101-122.

Olsen, N, R. Haagmans, T.J. Sabaka, A. Kuvshinov, S. Maus, M. Purucker, M.Rother, V. Lesur, and M Mandea (2006) The Swarm End-to-End mission simulator study: A demonstration of separating the various contributions to Earth's magnetic field using synthetic data, *Earth, Planets and Space*, 58(4), 359-370.

Parsons, T., J. McCarthy, W.M. Kohler, C.J. Ammon, H.M. Benz, J.A. Hole, and E.E. Criley (1996) Crustal structure of the Colorado Plateau, Arizona: Application of new long-offset seismic data analysis techniques, *J. Geophys. Res*., 101, 11173-11194.

Press, W.H., S.A. Teukolsky, W.T. Vetterling, and B.P. Flanney (1992) *Numerical Recipes in Fortran*: *The art of scientific computing*, 2nd edition, 963 pp, Cambridge University Press.

Purucker, M.E. (1990) The computation of vector magnetic anomalies: A comparison of techniques and errors, *Phys. Earth Plan. Int.*, 62, 231-245.

Purucker, M.E.,B. Langlais, N. Olsen, G. Hulot, and M. Mandea (2002) The southern edge of cratonic North America: Evidence from new satellite magnetometer observations, *Geophys. Res. Lett*, 29(15), doi:10.1029/2001GL013645.

Sabaka, T., N. Olsen, and M. Purucker (2004) Extending Comprehensive Models of the Earth's Magnetic Field with Oersted and CHAMP data, *Geophys. J. Int*.,159, 521-547.

Slavin, J.A., G. Le, R.J. Strangeway, Y. Wang, S.A.Boardsen, M.B. Moldwin, and H.E. Spence, Space Technology 5 multi-point measurements of near-Earth magnetic fields: Initial results, in press, *Geophysical Research Letters*.

Figure captions

Figure 1. a) Low altitude (<400 km) magnetic field gradients (nT/m) of the total anomaly field (Δ T) measured by ST-5 spacecraft 94 and 224 along descending orbits. These measured gradients exhibit a correlation coefficient with the CM4 model (Sabaka et al., 2004) in excess of 0.5. Spacecraft separation averaged 400 km (range 100-600). The CM4 fields used are the static fields between degrees 14-60, representing the lithospheric field. b) Low altitude magnetic field gradients, as in 1a, after a preliminary correction of the biases in the ST-5 gradient data. The correction entailed calculating, for each spacecraft, and for each pass, a median offset between the predicted and observed total anomaly field when the spacecraft is outside of the auroral zone. This median offset was used to correct the measured gradient. c) Predicted magnetic field gradients from CM4 at the same locations as measured in 1a above.

Figure 2. Stacked profile plots, showing measured total anomaly field (Δ T) and interspacecraft difference fields ($\hat{G} * d$), compared with those predicted by the Comprehensive (CM4) field model (Sabaka et al., 2004) over portions of North America covered by ST-5 observations at altitudes of less than 400 km. Red colors indicate positive fields or gradients, blue are negative.

Figure 3. MF-5 (Maus et al., 2007) model of total anomaly field (Δ T) at 400 km altitude (left), seismic crustal thickness (center) from Chulick and Mooney (2002), and magnetic

crustal thickness (right) inferred from seismic and magnetic data over one of the same portions of North America as shown in Figure 2. The magnetic crust is that part of the crust cooler than about 580 degrees C, the Curie temperature of magnetite. Boundaries of Colorado Plateau (CP) from Hunt (1956), and of Oligocene to early Miocene silicic volcanism unaffected by Tertiary extension (SI) on the Mexican mainland from Ferrari et al. (2002). The resolution of the magnetic crustal thickness map is dictated by the magnetic field map, and is approximately equal to 400 km. Hence, features such as the thickened crust of the Baja peninsula are resolvable, but the individual highs within the Baja peninsula are not. The black region in the Pacific south of Baja California has negative magnetic thicknesses, and suggests that unmodeled remanent magnetizations exist in this region.

Tables

Table 1. Residual statistics for total anomaly field (Δ T) and interspacecraft differences ($\hat{G} * d$) for ST-5 observations between March 28 and June 2, 2006. 094 and 224 are the two ST-5 spacecraft used in this analysis. Residuals are relative to the IGRF and static degrees 14-60 from CM4 (Sabaka et al., 2004).

Magnetic latitude northern boundary (degrees)	Observations (number)	RMS misfit (nT)	Type of observation	Maximum altitude (km)
90	331619	16.86	$\hat{G} * d$	400
70	263751	12.88	$\hat{G} * d$	400
60	177275	7.34	$\hat{G} * d$	400
50	112162	6.61	$\hat{G} * d$	400
90	331619	24.84	Δ T (094)	400
60	177275	14.66	Δ T (094)	400
50	112162	13.73	Δ T (094)	400
90	331619	25.42	Δ T (224)	400
60	177275	13.49	Δ T (224)	400
50	112162	10.92	Δ T (224)	400
90	754959	21.60	Δ T (224)	800
50	321778	12.32	Δ T (224)	800

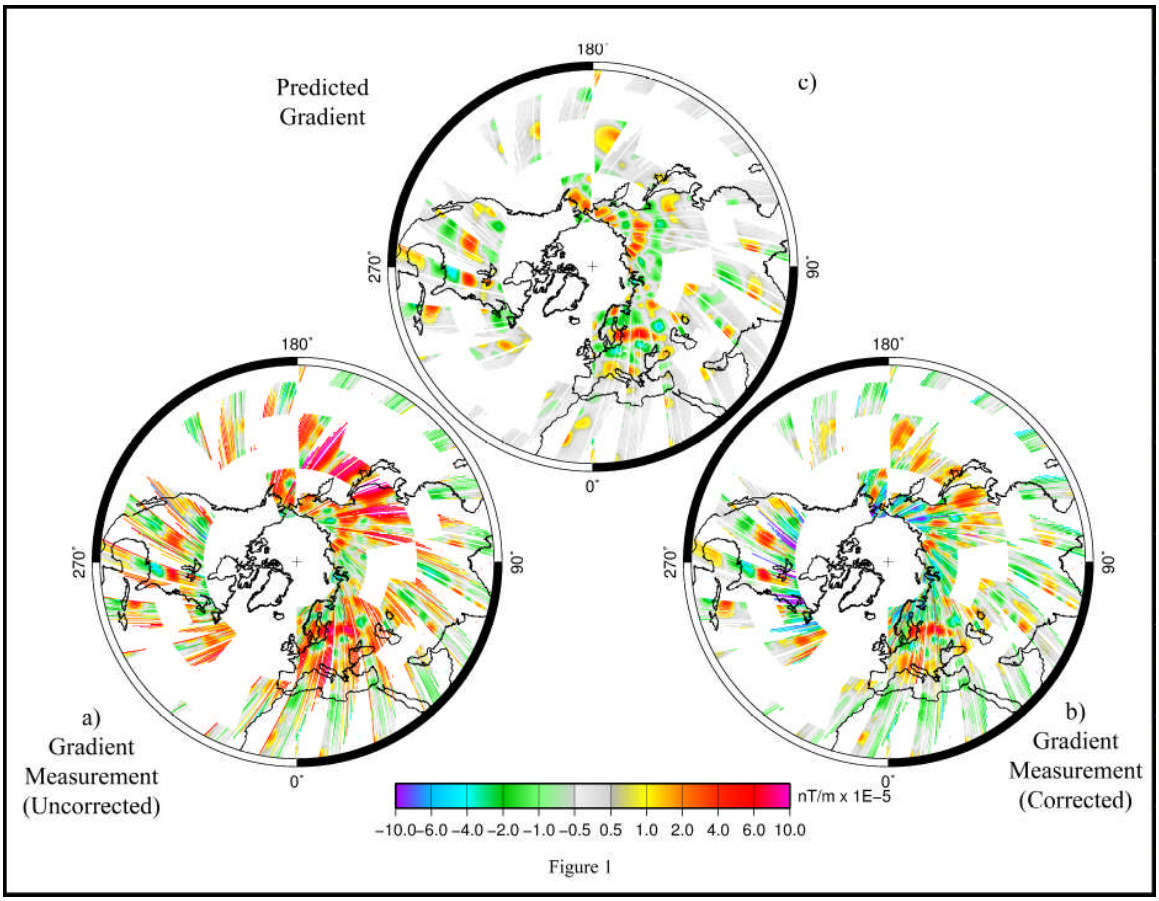
Predicted
Gradient
c)
180°
270°
90°
0°
180°
270°
90°
0°
180°
270°
90°
0°
a)
Gradient
Measurement
(Uncorrected)
b)
Gradient
Measurement
(Corrected)
nT/m x 1E–5
–10.0 –6.0 –4.0 –2.0 –1.0 –0.5 0.5 1.0 2.0 4.0 6.0 10.0

Figure 1

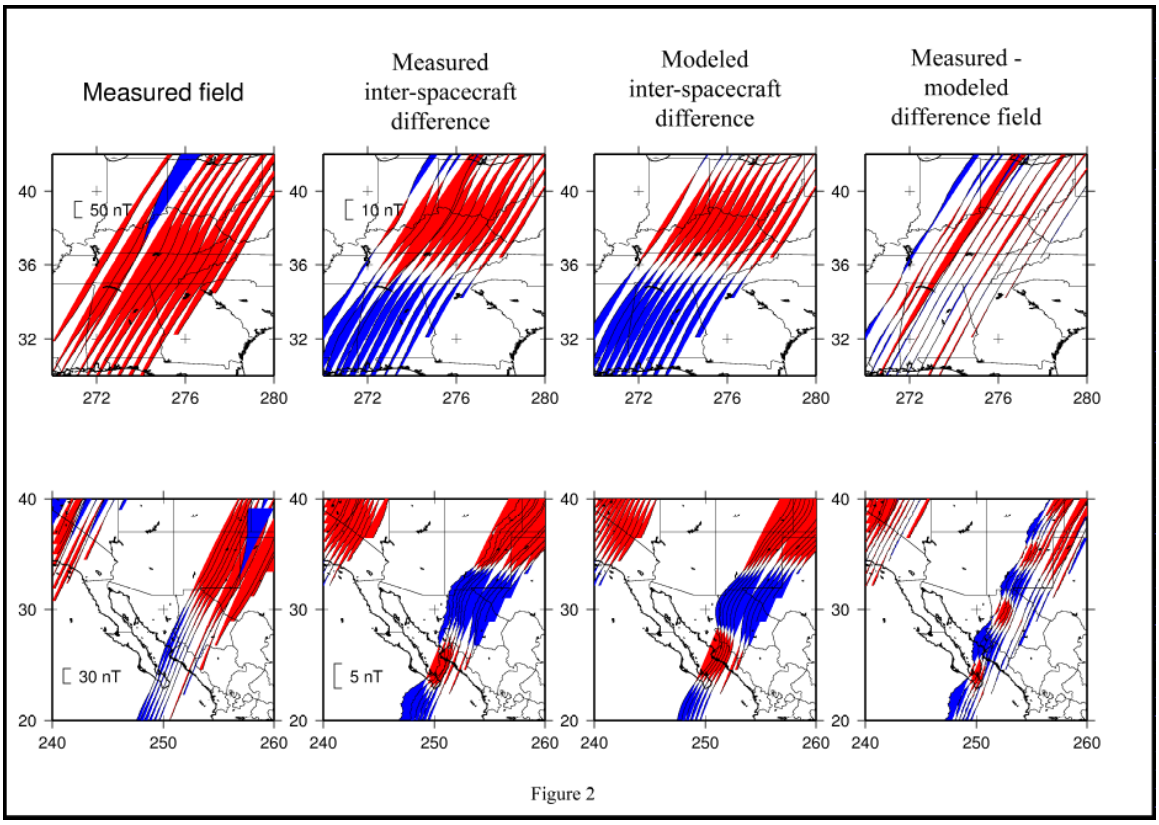

Figure 2

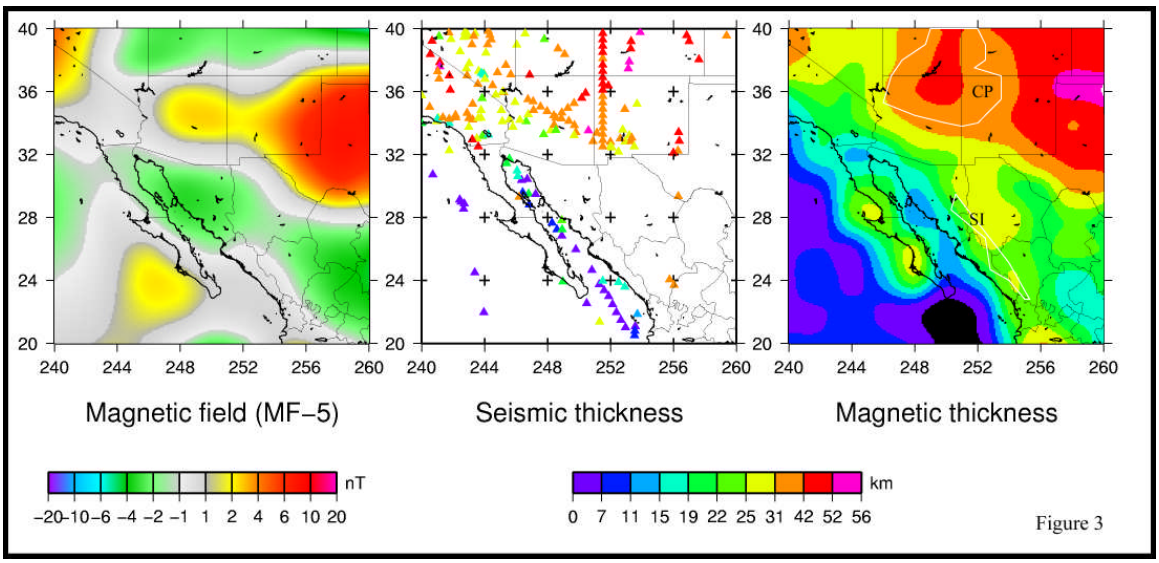

Figure 3